

Production of W^+W^- pairs via $\gamma^*\gamma^* \rightarrow W^+W^-$ subprocess with photon transverse momenta

Marta Łuszczak,^{1,*} Wolfgang Schäfer,^{2,†} and Antoni Szczurek^{2,‡}

¹ *Faculty of Mathematics and Natural Sciences,
University of Rzeszów, ul. Pigonia 1, PL-35-310 Rzeszów, Poland*

² *Institute of Nuclear Physics Polish Academy of Sciences,
ul. Radzikowskiego 152, PL-31-342 Cracow, Poland*

(Dated: October 11, 2018)

Abstract

We discuss production of W^+W^- pairs in proton-proton collisions induced by two-photon fusion including, for a first time, transverse momenta of incoming photons. The unintegrated inelastic fluxes (related to proton dissociation) of photons are calculated based on modern parametrizations of deep inelastic structure functions in a broad range of their arguments (x and Q^2). In our approach we can get separate contributions of different W helicities states. Several one- and two-dimensional differential distributions are shown and discussed. The present results are compared to the results of previous calculations within collinear factorization approach. Similar results are found except of some observables such as e.g. transverse momentum of the pair of W^+ and W^- . We find large contributions to the cross section from the region of large photon virtualities. We show decomposition of the total cross section as well as invariant mass distribution into the polarisation states of both W bosons. The role of the longitudinal F_L structure function is quantified. Its inclusion leads to a 4-5 % decrease of the cross section, almost independent of M_{WW} .

PACS numbers:

*Electronic address: luszczak@univ.rzeszow.pl

†Electronic address: Wolfgang.Schafer@ifj.edu.pl

‡Electronic address: antoni.szczurek@ifj.edu.pl

I. INTRODUCTION

Recently the partonic processes initiated by one or two photons in hadronic collisions at the Large Hadron Collider (LHC) are becoming an active field of research. The corresponding theoretical approach requires the calculation of photon fluxes in the proton-proton collision. The majority of practical approaches focused on a collinear factorization approach where the momentum of the colliding photon is collinear to the parent proton momentum. For a comprehensive review on photon-photon fusion reactions, see [1]. Recently, for the conditions of LHC, photon-photon fusion was discussed in the context of lepton pairs [2, 3], W^+W^- [4] or possible signals beyond the Standard Model, such as the production of charged Higgs bosons H^+H^- [5]. In Ref.[4] it was shown that photon-photon partonic processes are important for large invariant masses of W^+W^- pairs.

Several groups that provide the high-energy community with parton distribution functions included photons as partons in the proton [6–9], solving the corresponding coupled DGLAP evolution equations.

This strategy differs from the one adopted in Ref. [2, 3] (see also Ref.[10]), where following Ref. [1], the photon fluxes had been calculated in a data-driven way using their relation to the well-measured proton structure functions. Subsequently, such a data-driven approach was taken up in Refs. [11, 12].

The transverse momenta of photons were included so far only for $\gamma\gamma \rightarrow e^+e^-$ or $\gamma\gamma \rightarrow \mu^+\mu^-$ subprocesses [2, 3]. There we identified corners of phase space where transverse momenta of photons (or their virtualities) are large.

In the present paper we extend our studies to the production of W^+W^- pairs. We expect that here the virtualities of photons may be much larger than for l^+l^- production.

Particularly interesting is the region of large invariant masses of the W^+W^- system where the diphoton mechanism becomes one of the most important contributions for W^+W^- pair production. We shall compare the calculation within the k_T -factorization approach with those obtained previously in the collinear approximation. We shall discuss all types of processes as shown in Fig.1.

The $\gamma\gamma \rightarrow W^+W^-$ subprocess is interesting also in the context of searches of effects beyond Standard Model effects [13, 14], such as anomalous quartic gauge-boson couplings. First experimental studies on anomalous $\gamma\gamma WW$ couplings were already presented recently both by the CMS and ATLAS collaborations [15, 16]. We expect that our present estimate within the Standard Model will be therefore a useful reference point in searches beyond Standard Model. We shall also present a separate contribution for longitudinal W boson which is interesting in the context of WW final state interactions and/or searches for possible resonances, see for example [17–19].

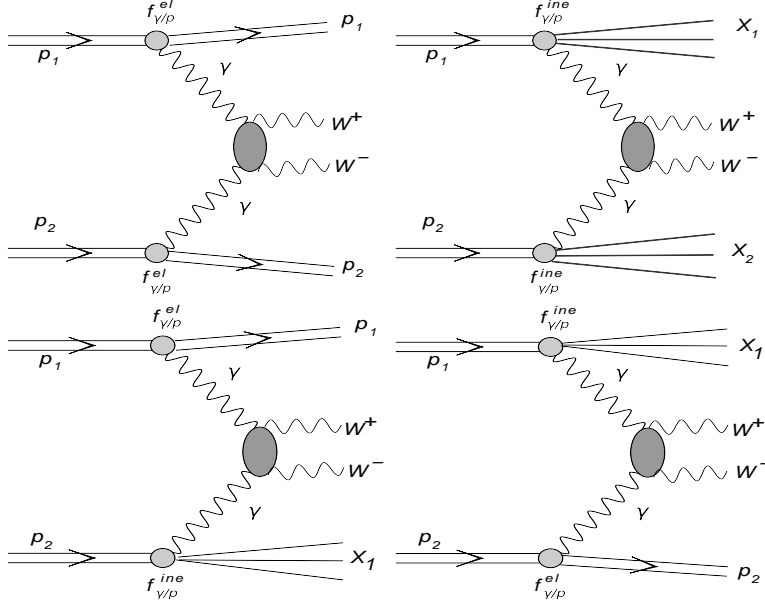


FIG. 1: Diagrams representing different categories of photon-photon induced mechanisms for production of W^+W^- pairs.

II. ACCOUNTING FOR TRANSVERSE MOMENTA OF PHOTONS

In this section we will include the transverse momentum of photons, so that the distributions of the transverse momentum of the W^+W^- pair and the azimuthal angle between the W 's have a nontrivial behaviour already at the lowest order. In [2, 3] a k_T -factorization approach for the $\gamma\gamma$ -fusion reactions in the high-energy limit of the pp -collision has been given. This approach has its domain of applicability in the region of small momentum fractions $z \ll 1$ carried by photons.

In this case, the unintegrated photon distributions can be calculated from the proton structure function $F_2(x, Q^2)$ alone in a data-driven way.

A broader range of applicability has the generalized equivalent-photon approximation of [1], in which a whole density matrix of photons appears. In some instances, for example when the masses squared of produced particles are much larger than the typical virtualities of photons, the density matrix simplifies and only transverse polarizations in the center-of-mass of colliding photons are important. We will adopt this approach for our numerical calculations of W^+W^- bosons below.

In both k_T -dependent approaches described above, the cross section for W^+W^- production can be written in the form

$$\frac{d\sigma^{(i,j)}}{dy_1 dy_2 d^2\vec{p}_{T1} d^2\vec{p}_{T2}} = \int \frac{d^2\vec{q}_{T1}}{\pi \vec{q}_{T1}^2} \frac{d^2\vec{q}_{T2}}{\pi \vec{q}_{T2}^2} \mathcal{F}_{\gamma^*/A}^{(i)}(x_1, \vec{q}_{T1}) \mathcal{F}_{\gamma^*/B}^{(j)}(x_2, \vec{q}_{T2}) \frac{d\sigma^*(p_1, p_2; \vec{q}_{T1}, \vec{q}_{T2})}{dy_1 dy_2 d^2\vec{p}_{T1} d^2\vec{p}_{T2}}, \quad (2.1)$$

where the indices $i, j \in \{\text{el}, \text{in}\}$ denote elastic or inelastic final states. The longitudinal momentum fractions of photons are obtained from the rapidities and transverse momenta

of final state W^+W^- as:

$$\begin{aligned} x_1 &= \sqrt{\frac{\vec{p}_{T1}^2 + m_W^2}{s}} e^{y_1} + \sqrt{\frac{\vec{p}_{T2}^2 + m_W^2}{s}} e^{y_2}, \\ x_2 &= \sqrt{\frac{\vec{p}_{T1}^2 + m_W^2}{s}} e^{-y_1} + \sqrt{\frac{\vec{p}_{T2}^2 + m_W^2}{s}} e^{-y_2}. \end{aligned} \quad (2.2)$$

For photons which carry transverse polarization in the $\gamma\gamma$ -cms frame, we write the relevant “off-shell” cross section as:

$$\frac{d\sigma^*(p_1, p_2; \vec{q}_{T1}, \vec{q}_{T2})}{dy_1 dy_2 d^2\vec{p}_{T1} d^2\vec{p}_{T2}} = \frac{1}{16\pi^2(x_1 x_2 s)^2} \sum_{\lambda_{W^+} \lambda_{W^-}} |M(\lambda_{W^+}, \lambda_{W^-})|^2 \delta^{(2)}(\vec{p}_{T1} + \vec{p}_{T2} - \vec{q}_{T1} - \vec{q}_{T2}), \quad (2.3)$$

where the matrix element M in terms of transverse momenta of incoming photons is given by

$$\begin{aligned} M(\lambda_{W^+} \lambda_{W^-}) &= \frac{1}{|\vec{q}_{\perp 1}| |\vec{q}_{\perp 2}|} \sum_{\lambda_1 \lambda_2} (\vec{e}_{\perp}(\lambda_1) \cdot \vec{q}_{\perp 1}) (\vec{e}_{\perp}^*(\lambda_2) \cdot \vec{q}_{\perp 2}) \mathcal{M}(\lambda_1, \lambda_2; \lambda_{W^+}, \lambda_{W^-}) \\ &= \frac{1}{|\vec{q}_{\perp 1}| |\vec{q}_{\perp 2}|} \sum_{\lambda_1 \lambda_2} q_{\perp 1}^i q_{\perp 2}^j e_i(\lambda_1) e_j^*(\lambda_2) \cdot \mathcal{M}(\lambda_1, \lambda_2; \lambda_{W^+}, \lambda_{W^-}), \end{aligned} \quad (2.4)$$

with $\vec{e}_{\perp}(\lambda) = -i(\lambda \vec{e}_x + i \vec{e}_y)$. The helicity matrix elements $\mathcal{M}(\lambda_1, \lambda_2; \lambda_{W^+}, \lambda_{W^-})$ for the process $\gamma(\lambda_1) \gamma(\lambda_2) \rightarrow W^+(\lambda_{W^+}) W^-(\lambda_{W^-})$ are taken from Ref. [20], where one can also find explicit helicity states defined in the cm-frame of the W^+W^- pair. It is useful to decompose the matrix element further, using the identity

$$\begin{aligned} q_{\perp 1}^i q_{\perp 2}^j &= \frac{1}{2} \delta_{ij} (\vec{q}_{\perp 1} \cdot \vec{q}_{\perp 2}) + \frac{1}{2} (q_{\perp 1}^i q_{\perp 2}^j + q_{\perp 1}^j q_{\perp 2}^i - \delta_{ij} (\vec{q}_{\perp 1} \cdot \vec{q}_{\perp 2})) + \frac{1}{2} (q_{\perp 1}^i q_{\perp 2}^j - q_{\perp 1}^j q_{\perp 2}^i) \\ &= \frac{1}{2} \delta_{ij} (\vec{q}_{\perp 1} \cdot \vec{q}_{\perp 2}) + \frac{1}{2} t_{ij}^{kl} q_{\perp 1}^k q_{\perp 2}^l + \frac{1}{2} \epsilon_{ij} [\vec{q}_{\perp 1}, \vec{q}_{\perp 2}]. \end{aligned} \quad (2.5)$$

Here the antisymmetric symbol is defined by $\epsilon_{xy} = -\epsilon_{yx} = 1$, and

$$[\vec{q}_{\perp 1}, \vec{q}_{\perp 2}] \equiv q_{\perp 1}^x q_{\perp 2}^y - q_{\perp 1}^y q_{\perp 2}^x, \quad (2.6)$$

furthermore

$$t_{ij}^{kl} = \delta_i^k \delta_j^l + \delta_j^k \delta_i^l - \delta_j^i \delta_l^k. \quad (2.7)$$

We then obtain for the helicity-matrix element

$$\begin{aligned} M(\lambda_{W^+} \lambda_{W^-}) &= \frac{1}{|\vec{q}_{\perp 1}| |\vec{q}_{\perp 2}|} \left\{ (\vec{q}_{\perp 1} \cdot \vec{q}_{\perp 2}) \cdot \left(\mathcal{M}(++; \lambda_{W^+} \lambda_{W^-}) + \mathcal{M}(--; \lambda_{W^+} \lambda_{W^-}) \right) \right. \\ &\quad - i [\vec{q}_{\perp 1}, \vec{q}_{\perp 2}] \left(\mathcal{M}(++; \lambda_{W^+} \lambda_{W^-}) - \mathcal{M}(--; \lambda_{W^+} \lambda_{W^-}) \right) \\ &\quad - (q_{\perp 1}^x q_{\perp 2}^x - q_{\perp 1}^y q_{\perp 2}^y) \left(\mathcal{M}(+-; \lambda_{W^+} \lambda_{W^-}) + \mathcal{M}(-+; \lambda_{W^+} \lambda_{W^-}) \right) \\ &\quad \left. - i (q_{\perp 1}^x q_{\perp 2}^y + q_{\perp 1}^y q_{\perp 2}^x) \left(\mathcal{M}(+-; \lambda_{W^+} \lambda_{W^-}) - \mathcal{M}(-+; \lambda_{W^+} \lambda_{W^-}) \right) \right\}. \end{aligned} \quad (2.8)$$

Together with these matrix elements, we use the photon fluxes from [1]. We write the photon distribution differentially as

$$dn^{\text{in,el}} = \frac{dz}{z} \frac{d^2 \vec{q}_T}{\pi \vec{q}_T^2} \mathcal{F}_{\gamma^* \leftarrow p}^{\text{in,el}}(z, \vec{q}_T). \quad (2.9)$$

The virtuality Q^2 of the photon carrying momentum fraction z and transverse momentum \vec{q}_T is

$$Q^2 = \frac{\vec{q}_T^2 + z(M_X^2 - m_p^2) + z^2 m_p^2}{(1-z)}, \quad (2.10)$$

where M_X is the invariant mass of the proton remnant in the final state. Then using

$$\frac{dQ^2}{Q^2} = \frac{Q^2 - Q_{\text{min}}^2}{Q^2} \frac{d^2 \vec{q}_T}{\pi \vec{q}_T^2}, \text{ and } \frac{\vec{q}_T^2}{\vec{q}_T^2 + z(M_X^2 - m_p^2) + z^2 m_p^2} = \frac{Q^2 - Q_{\text{min}}^2}{Q^2}, \quad (2.11)$$

we can write the fluxes from [1] as

$$\begin{aligned} \mathcal{F}_{\gamma^* \leftarrow p}^{\text{in}}(z, \vec{q}_T) = & \frac{\alpha_{\text{em}}}{\pi} \left\{ (1-z) \left(\frac{\vec{q}_T^2}{\vec{q}_T^2 + z(M_X^2 - m_p^2) + z^2 m_p^2} \right)^2 \frac{F_2(x_{\text{Bj}}, Q^2)}{Q^2 + M_X^2 - m_p^2} \right. \\ & \left. + \frac{z^2}{4x_{\text{Bj}}^2} \frac{\vec{q}_T^2}{\vec{q}_T^2 + z(M_X^2 - m_p^2) + z^2 m_p^2} \frac{2x_{\text{Bj}} F_1(x_{\text{Bj}}, Q^2)}{Q^2 + M_X^2 - m_p^2} \right\}, \end{aligned} \quad (2.12)$$

and similarly for the elastic piece

$$\begin{aligned} \mathcal{F}_{\gamma^* \leftarrow p}^{\text{el}}(z, \vec{q}_T) = & \frac{\alpha_{\text{em}}}{\pi} \left\{ (1-z) \left(\frac{\vec{q}_T^2}{\vec{q}_T^2 + z(M_X^2 - m_p^2) + z^2 m_p^2} \right)^2 \frac{4m_p^2 G_E^2(Q^2) + Q^2 G_M^2(Q^2)}{4m_p^2 + Q^2} \right. \\ & \left. + \frac{z^2}{4} \frac{\vec{q}_T^2}{\vec{q}_T^2 + z(M_X^2 - m_p^2) + z^2 m_p^2} G_M^2(Q^2) \right\}. \end{aligned} \quad (2.13)$$

These fluxes differ from the ones from Ref. [2, 3], which apply in the high energy limit. The difference in these approaches is threefold: firstly, fluxes in Ref. [2, 3] also include a contribution from longitudinal polarizations of photons in the $\gamma^* \gamma^*$ cms, secondly within the accuracy of the high-energy limit, the fluxes of [2, 3] depend on $F_2(x_{\text{Bj}}, Q^2)$ only, and thirdly these fluxes must be accompanied by the corresponding off-shell matrix element. Notice that in (2.12) instead of $F_2(x_{\text{Bj}}, Q^2)$, $F_1(x_{\text{Bj}}, Q^2)$, one may use the pair $F_2(x_{\text{Bj}}, Q^2)$, $F_L(x_{\text{Bj}}, Q^2)$, where

$$F_L(x_{\text{Bj}}, Q^2) = \left(1 + \frac{4x_{\text{Bj}}^2 m_p^2}{Q^2} \right) F_2(x_{\text{Bj}}, Q^2) - 2x_{\text{Bj}} F_1(x_{\text{Bj}}, Q^2) \quad (2.14)$$

is the longitudinal structure function of the proton.

III. COLLINEAR-FACTORIZATION APPROACH

In some cases it can be sufficient to neglect the transverse momenta of partons. Then photons are treated as collinear partons in a proton. Like other parton densities, the photon distribution $\gamma(z, \mu^2)$ is a function of the longitudinal momentum fraction z carried by the photon and the factorization scale μ^2 of the hard process the photon participates in.

A number of parametrizations of the photon parton distributions have become available recently [6–9, 11, 12]. Most of them are based on including photons into the coupled DGLAP evolution equations for quarks and gluons [6–9] and attempt to extract the photon distributions from either global fits or fits to processes that are deemed to have a strong sensitivity to the photon distribution. A different approach is taken in Ref.[11, 12], where similarly to Ref.[3] a data driven approach is taken. An explicit coherent contribution is related to the electromagnetic form factors of a proton. A second contribution is related to the proton structure functions F_2 and F_L .

In the collinear approach the photon-photon contribution to inclusive cross section for W^+W^- production can be written as:

$$\frac{d\sigma^{(i,j)}}{dy_1 dy_2 d^2p_T} = \frac{1}{16\pi^2(x_1 x_2 s)^2} \sum_{i,j} x_1 \gamma^{(i)}(x_1, \mu^2) x_2 \gamma^{(j)}(x_2, \mu^2) \overline{|\mathcal{M}_{\gamma\gamma \rightarrow W^+W^-}|^2}. \quad (3.1)$$

Here

$$\begin{aligned} x_1 &= \sqrt{\frac{p_T^2 + m_W^2}{s}} \left(\exp(y_1) + \exp(y_2) \right), \\ x_2 &= \sqrt{\frac{p_T^2 + m_W^2}{s}} \left(\exp(-y_1) + \exp(-y_2) \right). \end{aligned} \quad (3.2)$$

Above indices i and j denote $i, j = \text{el, in}$, i.e. they correspond to elastic or inelastic components similarly as for the k_T -factorization discussed in section II above. The factorization scale is chosen as $\mu^2 = m_T^2 = p_T^2 + m_W^2$.

Calculations with collinear partons from eq. 3.1 have the drawback, that at the lowest order the produced two-body system is strictly in back-to-back kinematics. Consequently the distribution in transverse momentum of the produced pair is a delta-function. Similarly behaved the distribution of the azimuthal angle $\Delta\phi$ between the produced particles, which is a delta function centered at $\Delta\phi = \pi$.

It should be made clear, however, that in Monte-Carlo simulations of the inclusive W^+W^- -pair production, collinear cross sections, such as the one given by (3.1) can be embedded into events including e.g. initial state emissions from parton showers, which will give a finite transverse momentum to the W^+W^- -pair. The effect of highly virtual photons must then be accounted for by matching to higher order processes such as e.g. $q\gamma \rightarrow qW^+W^-$ or $qq \rightarrow qqW^+W^-$. The necessary rather sophisticated computational techniques are described e.g. in [21]. We are not aware of calculations of the processes of interest here in this approach and prefer to stick to the more straightforward k_T -factorization described in the previous section. Also, it should be noted that when we refer to the collinear approximation in the remainder of the text, we always refer to calculations from Eq.(3.1).

IV. RESULTS

In this section we shall show our results for the k_T -factorization approach. We shall concentrate first on the inelastic-inelastic contribution (see Fig.1). In the present paper we will not include experimental cuts but rather consider full phase space calculations.

We start from showing the cross sections using different parametrizations of proton structure functions.

Here we use the following options:

1. the Abramowicz-Levy-Levin-Maor fit [22, 23] used previously also in [3], abbreviated here ALLM.
2. a newly constructed parametrization, which at $Q^2 > 9 \text{ GeV}^2$ uses an NNLO calculation of F_2 and F_L from NNLO MSTW 2008 partons [27]. It employs a useful code by the MSTW group [27] to calculate structure functions. At $Q^2 > 9 \text{ GeV}^2$ this fit uses the parametrization of Bosted and Christy [24] in the resonance region, and a version of the ALLM fit published by the HERMES Collaboration [25] for the continuum region. It also uses information on the longitudinal structure function from SLAC [26]. As the fit is constructed closely following the LUXqed work Ref.[12], we call this fit LUX-like.
3. a Vector-Meson-Dominance model inspired fit of F_2 proposed in [28] at low Q^2 , which is completed by the same NNLO MSTW structure function as above at large Q^2 . This fit is labelled SU for brevity.

One can see from Table I that the largest inelastic-inelastic component is in all calculations systematically bigger than the elastic-elastic component, which gives the smallest contribution. For the case of production of e^+e^- or $\mu^+\mu^-$ via $\gamma\gamma$ fusion all components were of the same size [3].

We obtain cross sections of about 0.8–1 pb at $\sqrt{s} = 8 \text{ TeV}$ and 1.5–1.8 pb at $\sqrt{s} = 13 \text{ TeV}$. This may be compared to $41.1 \pm 15.3 \text{ (stat)} \pm 5.8 \text{ (syst)} \pm 4.5 \text{ (lumi) pb}$ (CMS [30]) and $54.4 \pm 4.0 \text{ (stat)} \pm 3.9 \text{ (syst)} \pm 2.0 \text{ (lumi) pb}$ (ATLAS [31]) measured (and extrapolated) at the LHC for $\sqrt{s} = 7 \text{ TeV}$. This shows that the two-photon production constitutes about 2 % of the total cross section. However, its relative contribution, as will be discussed below, increases with M_{WW} .

A. One-dimensional distributions

In Fig.2 we show invariant mass distributions for $\sqrt{s} = 8 \text{ TeV}$ (left panel) and $\sqrt{s} = 13 \text{ TeV}$ (right panel). The calculations have been performed with different parametrizations of structure functions including the LUX-like one. There are large uncertainties in the region of large invariant masses. The uncertainties become smaller for larger \sqrt{s} . We will compare to Ref.[4], i.e. to result of collinear calculations with the rather old MRST04 QED set [6] (dash-dotted line). The new results should be regarded as an update of the older results in [4].

The distribution in transverse momentum of a W boson is shown in Fig.3. At low transverse momenta there is a relatively small theoretical uncertainty. The result obtained with our LUX-like structure function should be considered as our best estimate.

contribution	8 TeV	13 TeV
LUX-like		
$\gamma_{el}\gamma_{in}$	0.214	0.409
$\gamma_{in}\gamma_{el}$	0.214	0.409
$\gamma_{in}\gamma_{in}$	0.478	1.090
ALLM97 F2		
$\gamma_{el}\gamma_{in}$	0.197	0.318
$\gamma_{in}\gamma_{el}$	0.197	0.318
$\gamma_{in}\gamma_{in}$	0.289	0.701
SU F2		
$\gamma_{el}\gamma_{in}$	0.192	0.420
$\gamma_{in}\gamma_{el}$	0.192	0.420
$\gamma_{in}\gamma_{in}$	0.396	0.927
LUXqed collinear		
$\gamma_{in+el} \gamma_{in+el}$	0.366	0.778
MRST04 QED collinear		
$\gamma_{el}\gamma_{in}$	0.171	0.341
$\gamma_{in}\gamma_{el}$	0.171	0.341
$\gamma_{in}\gamma_{in}$	0.548	0.980
Elastic- Elastic		
$\gamma_{el}\gamma_{el}$ (Budnev)	0.130	0.273
$\gamma_{el}\gamma_{el}$ (DZ)	0.124	0.267

TABLE I: Cross sections (in pb) for different contributions and different F2 structure functions: LUX, ALLM97 and SU, compared to the relevant collinear distributions with MRST04 QED and LUXqed distributions. The elastic-elastic contributions were obtained using fluxes from Refs. [1], [29].

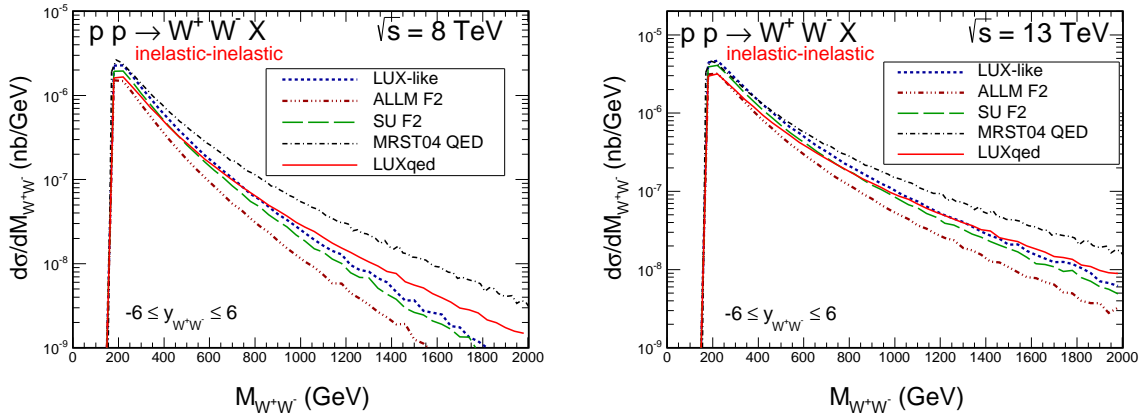


FIG. 2: The inelastic-inelastic contribution to W^+W^- invariant mass distributions for different structure functions: LUX-like, ALLM97, SU compared to the relevant collinear distributions: MRST04 QED, LUXqed. The left panel shows results for $\sqrt{s} = 8$ TeV, while the right panel shows results for $\sqrt{s} = 13$ TeV.

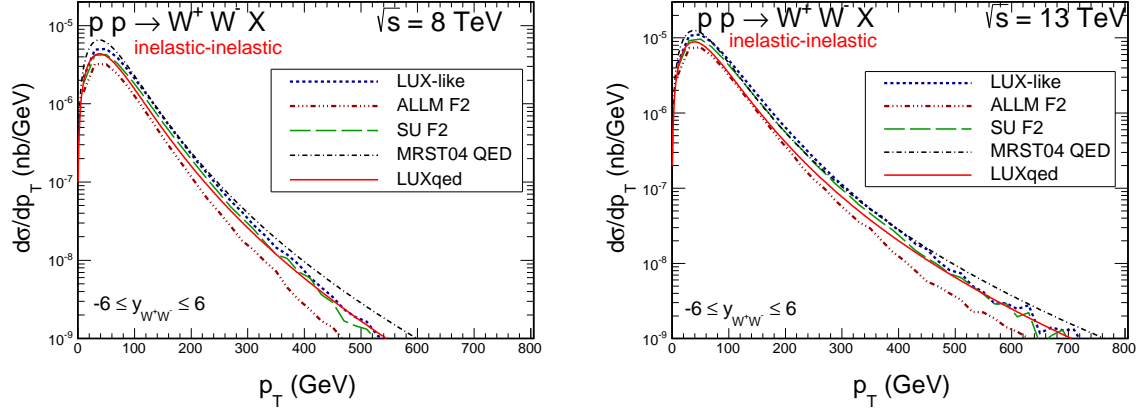


FIG. 3: Transverse momentum distribution of W^+ or W^- bosons for different structure functions: LUX-like, ALLM97, SU compared to the relevant collinear distributions: MRST04 QED, LUXqed. The left panel shows results for $\sqrt{s} = 8$ TeV, while the right panel shows results for $\sqrt{s} = 13$ TeV.

For completeness we show also rapidity distributions of W^+/W^- bosons in Fig.4. The distribution in collinear approach extends to much larger rapidities, especially for $\sqrt{s} = 13$ TeV.

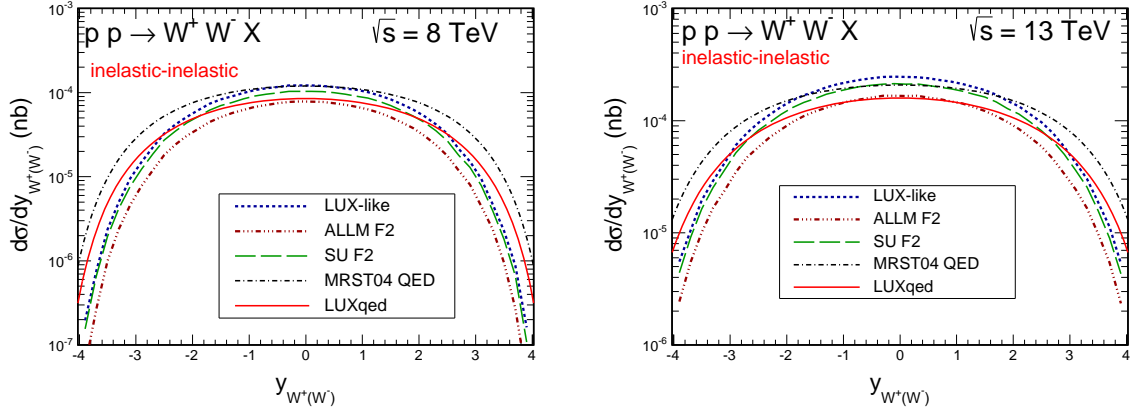


FIG. 4: Rapidity distribution of W^+ or W^- bosons for different structure functions: LUX-like, ALLM97, SU. The left panel shows results for the $\sqrt{s} = 8$ TeV, while the right panel shows results for $\sqrt{s} = 13$ TeV.

In Fig.5 we show distribution in transverse momentum of the W^+W^- pair, $p_{T,sum}$. Quite large pair transverse momenta are possible. In contrast in leading-order using collinear partons, the corresponding distribution is just a Dirac delta function at $p_{T,sum} = 0$. The k_T -factorization approach should be therefore here a much better approach. This distribution is, however, a bit academic as in practice one measures only charged leptons and the neutrinos escape experimental observation, but the figure demonstrates theoretical preference of the k_T -factorization approach over the collinear approach. The nonvanishing pair transverse momentum can influence the transverse momentum distributions of associated leptons (usually μ^+e^- or μ^-e^+) when it is large. This effect will be discussed elsewhere.

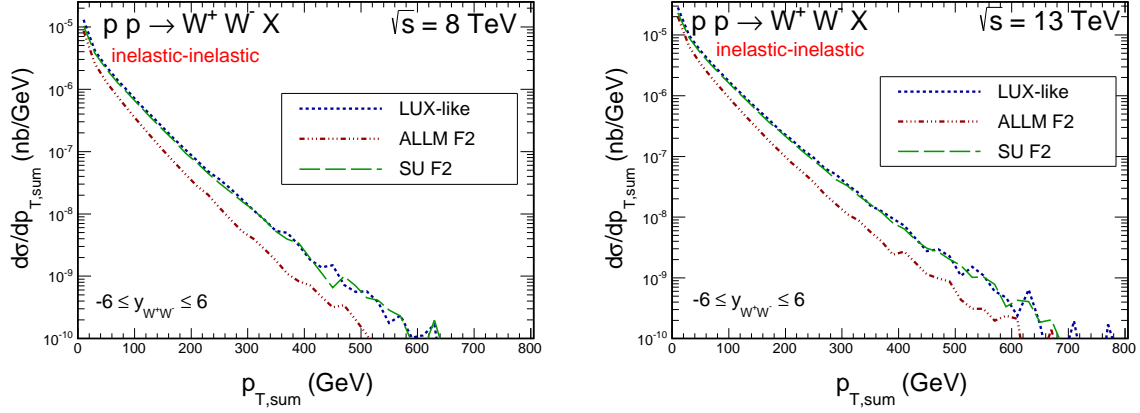


FIG. 5: Transverse momentum distribution of W^+W^- bosons for different structure functions: LUX-like, ALLM97, SU. The left panel shows results for $\sqrt{s} = 8$ TeV, while the right panel shows results for $\sqrt{s} = 13$ TeV.

Our approach also goes beyond [11, 12] in that it allows us to obtain the distribution of the mass of the proton remnant(s). These distributions are shown in Fig.6. Quite large masses of the remnant system are generated. Notice, that the larger is the invariant mass, the smaller is the rapidity gap from the proton remnant to the WW system. Detailed studies of this effect require a hadronisation of the remnant system, which goes beyond the scope of the present paper.

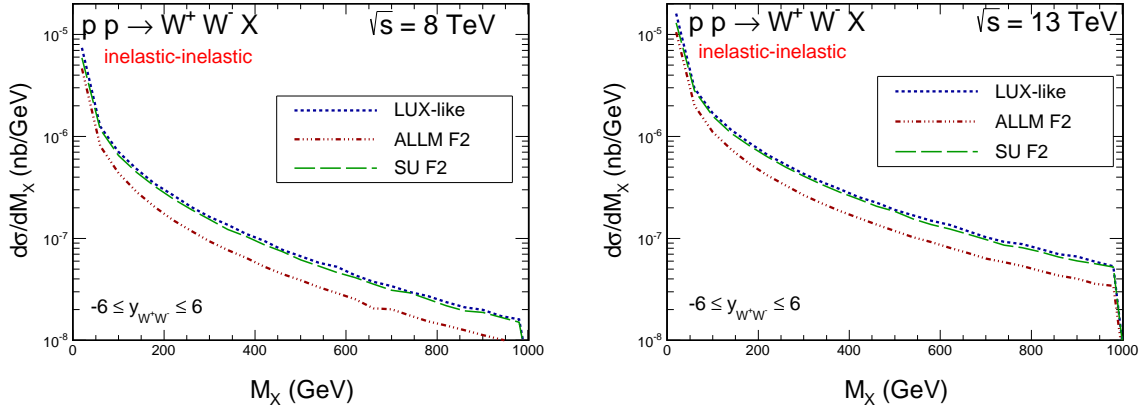


FIG. 6: Missing mass distributions for inelastic-inelastic photon-photon contributions for different parametrizations of the structure functions as explained inside the figures for two energies: $\sqrt{s} = 8$ TeV (left panel) and $\sqrt{s} = 13$ TeV (right panel).

Now we shall compare results corresponding to different diagrams shown in Fig.1. We start by showing distributions in invariant mass (see Fig.7). The inelastic contributions (inelastic-inelastic, inelastic-elastic or elastic-inelastic) are larger than the purely elastic (elastic-elastic) contribution. For reference we show distributions in the collinear approach with the LUXqed structure function parametrization.

In Fig.8 we compare transverse momentum distributions for all components of Fig.1. Similar slopes are obtained for different components, while the corresponding cross sections

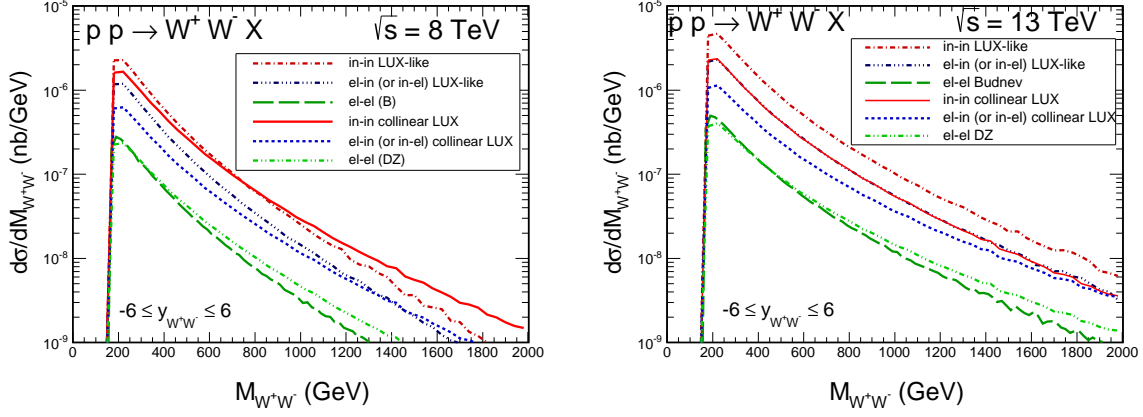


FIG. 7: The inelastic-inelastic, elastic-inelastic, inelastic-elastic and elastic-elastic contributions to W^+W^- invariant mass distributions for the k_T -factorization approach with the LUX-like structure function compared to the relevant distribution for collinear approach with similar structure function LUXqed. The left panel shows results for $\sqrt{s} = 8$ TeV, while the right panel shows results for $\sqrt{s} = 13$ TeV.

are different.

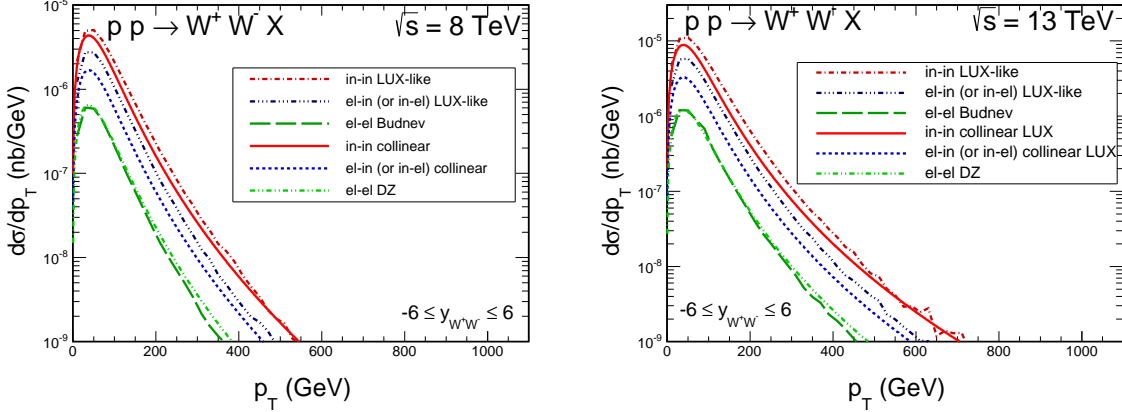


FIG. 8: Transverse momentum distribution of W^+ or W^- bosons for the inelastic-inelastic, elastic-inelastic, inelastic-elastic and elastic-elastic contributions for LUX-like structure function compared to the relevant distribution for collinear approach with the LUXqed. The left panel shows results for $\sqrt{s} = 8$ TeV, while the right panel shows results for $\sqrt{s} = 13$ TeV.

A similar result for the pair transverse momentum distribution is shown in Fig.8. The distribution for the inelastic-inelastic contribution is broader than that for elastic-inelastic or inelastic-elastic component. The elastic-elastic contribution gives very narrow distribution compared to the two other components.

The missing mass distributions for different components are shown in Fig.10. The shape for the elastic-inelastic and inelastic-elastic is the same as that for inelastic-inelastic component. The one for the elastic-elastic contribution is just the Dirac delta function at $M_X = M_Y = m_p$. We shall return to the issue whether the distributions in M_X and M_Y for

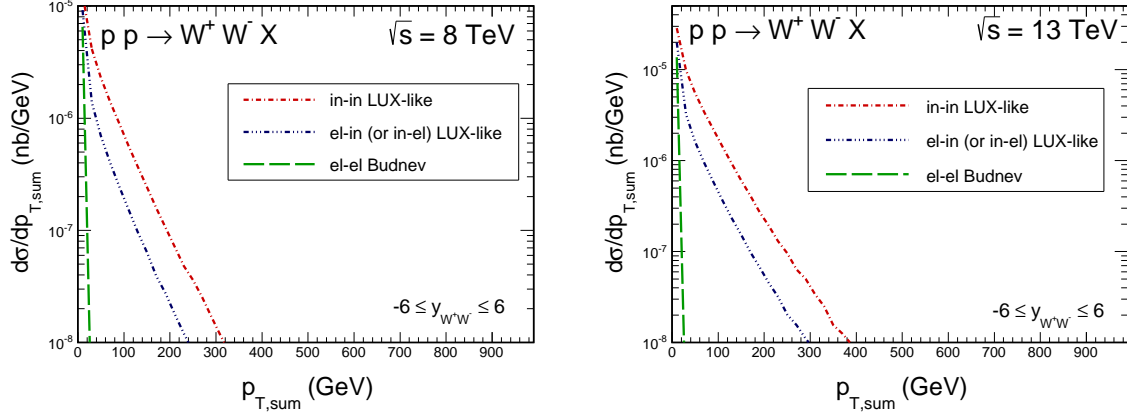


FIG. 9: Distribution in transverse momentum of the W^+W^- pairs for the inelastic-inelastic, elastic-inelastic, inelastic-elastic and elastic-elastic contributions for the LUX-like structure function. The left panel shows results for $\sqrt{s} = 8$ TeV, while the right panel shows results for $\sqrt{s} = 13$ TeV.

the inelastic-inelastic component are correlated when discussing two-dimensional distributions of correlation character.

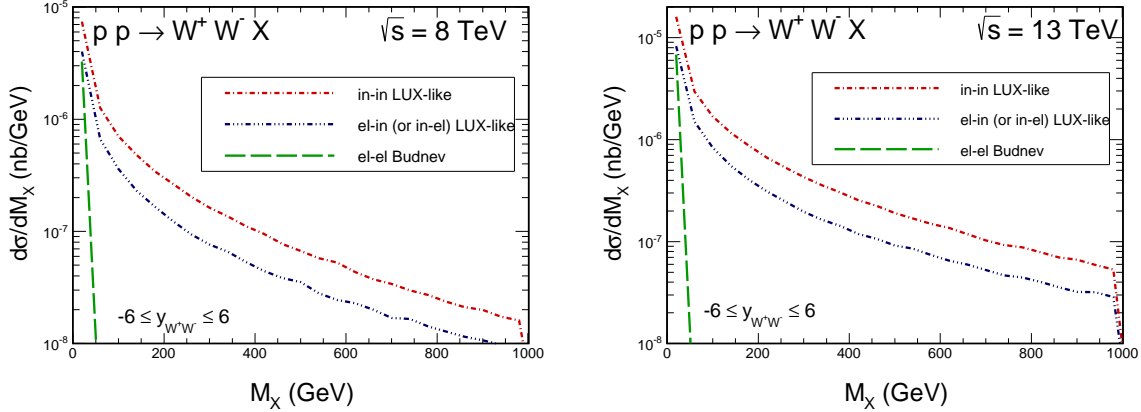


FIG. 10: Missing mass distributions for the inelastic-inelastic, elastic-inelastic, inelastic-elastic and elastic-elastic contributions for the LUX-like structure function. The left panel shows results for $\sqrt{s} = 8$ TeV, while the right panel shows results for $\sqrt{s} = 13$ TeV.

B. Correlation observables

Now we shall proceed to two-dimensional distributions of correlation character.

In the collinear approximation, the incoming photons are taken to be on-mass shell, i.e. massless. How the situation changes in our approach will be discussed in the following. In Fig.11 we show distribution in $Q_1^2 \times Q_2^2$ (please note logarithmic scales on both axes). A plateau extending to $Q_1^2, Q_2^2 \sim 10^4$ GeV can be seen. The result shows that collinear-factorization approach could be far from being realistic for the W^+W^- production, at least

in some parts of the phase space.

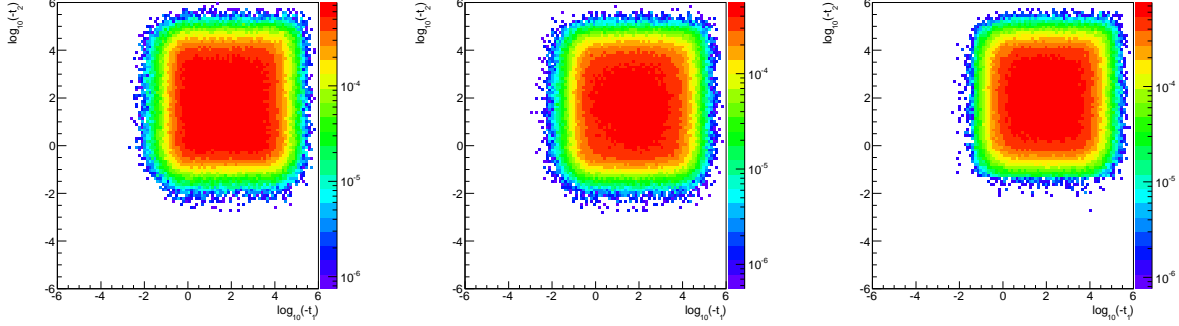


FIG. 11: Distributions for $Q_1^2 \times Q_2^2$ for different structure functions: LUX-like, ALLM97, SU for $\sqrt{s} = 13$ TeV.

In Fig.12 we discuss correlation between $t_1 = -Q_1^2$ or $t_2 = -Q_2^2$ and invariant mass of the W^+W^- system produced in the photon-photon fusion (please note logarithmic scale in rapidity). At large M_{WW} there are no small virtualities of photons. Therefore the collinear-factorization approach may be expected to be better close to the threshold and worse for large WW invariant masses. This may be important in establishing a reference Standard Model result in the studies searching for effects beyond Standard Model. The result does not depend on the parametrization of the structure function.

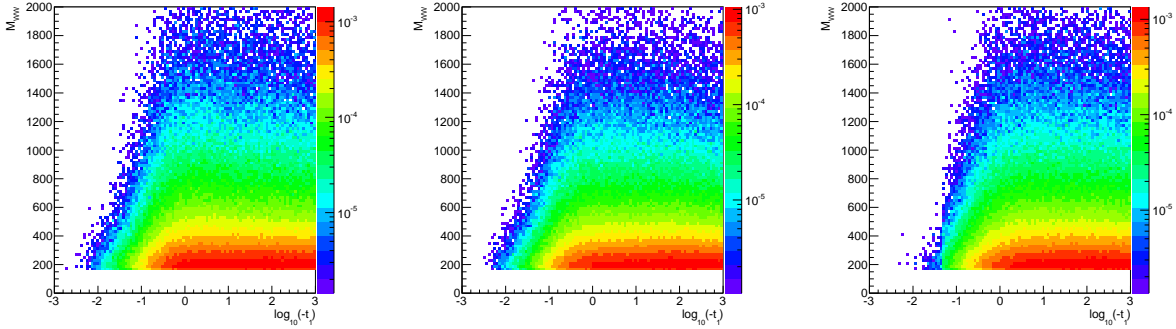


FIG. 12: Distributions in $Q_1^2 \times M_{WW}$ (or $Q_2^2 \times M_{WW}$) for different structure functions: LUX-like, ALLM97, SU for $\sqrt{s} = 13$ TeV.

In the inelastic-inelastic case both protons undergo dissociation into a complicated final state. What happens to the remnant systems will be discussed elsewhere. Here we show whether the photon virtualities and Bjorken- x values (arguments of the structure functions) are correlated. Only a small correlation can be observed. The figure shows that rather large Bjorken- x give the dominant contribution. This is region corresponding to fixed-target experiments performed in 80ies and 90ies.

For completeness in Fig.14 we show potential correlations in masses of both dissociated systems. The maximum of the two-dimensional distribution occurs when M_X, M_Y are rather small. When one of the masses is large the second is typically small. So we typically expect situations with small rapidity gap on one side and large gap on the other side of the “centrally” produced W^+W^- system. This will be discussed in detail elsewhere.

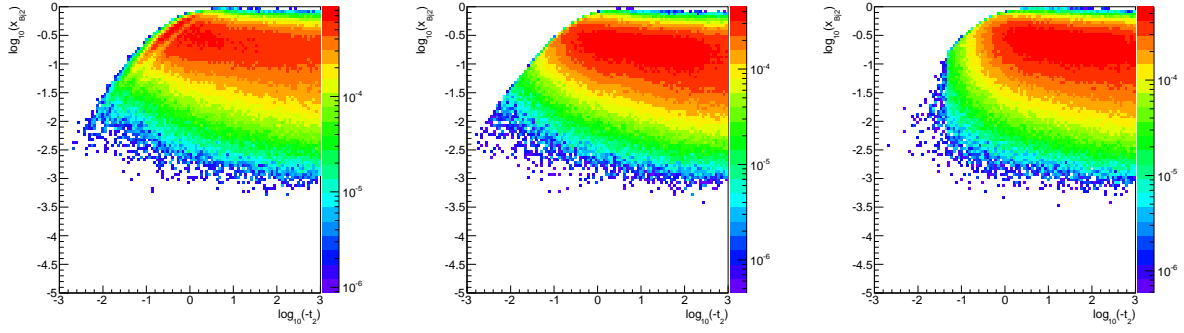


FIG. 13: Correlations in $Q_{1/2}^2 \times x_{1/2}$ for different F_2 structure functions: LUX-like, ALLM97, SU for $\sqrt{s} = 13$ TeV.

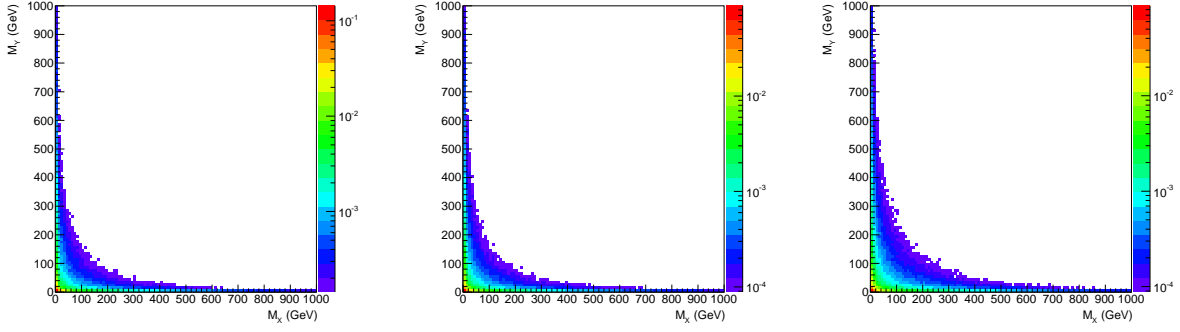


FIG. 14: Correlations in masses of the remnant systems for the double inelastic contribution for three different F_2 structure functions: LUX-like, ALLM97, SU for $\sqrt{s} = 13$ TeV.

C. Decomposition into polarization components

The matrix elements in Eq.(2.8) allow to calculate cross sections for different states of polarization of W bosons (polarizations here are defined in the W^+W^- center-of-mass frame, for explicit formulas, see [20]). It can be seen that the TT (both W 's are transversely polarized) component is larger than 80 %. The LL (both W 's longitudinally polarized) component plays a special role in studies of WW interactions. However in the photon-photon fusion the cross section for production of this component is smaller than 5 % of the total cross section.

To make a thorough study of possible effects beyond the SM in the LL channel, one should include decays of W 's. Then, the small LL component can be enhanced by interference with transverse W 's.

In fact it is more interesting what happens at large WW invariant masses $M_{WW} > 1$ TeV where effect beyond Standard Model could show up. In Fig.15 we show the decomposition into different polarization states of W bosons as a function of the WW invariant mass. We observe that the TT component dominates in the whole invariant mass region.

contribution	8 TeV	13 TeV
TT	0.405	0.950
LL	0.017	0.046
LT + TL	0.028 + 0.028	0.052 + 0.052
SUM	0.478	1.090

TABLE II: Contributions of different polarizations of W bosons for the inelastic-inelastic component for the LUX-like structure function. The cross sections are given in pb .

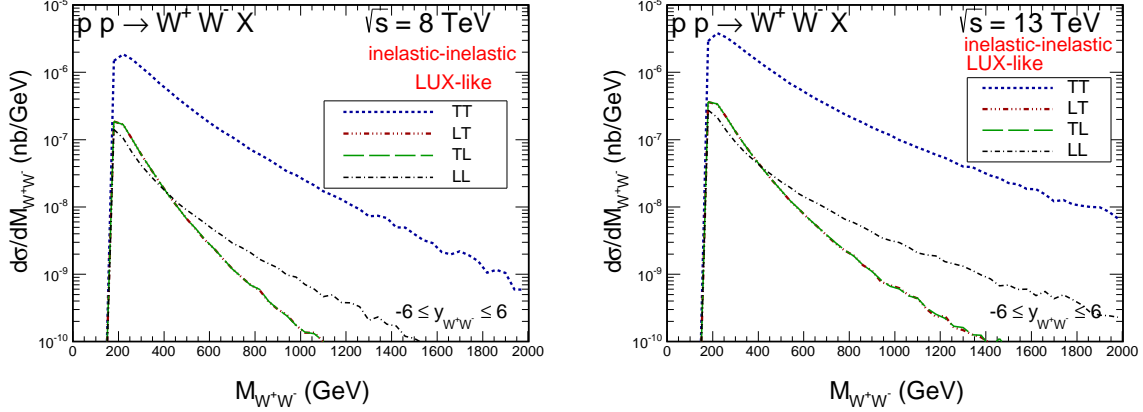


FIG. 15: Decomposition into polarization states of W bosons for the inelastic-inelastic component as a function of M_{WW} . The calculation was performed for the LUX-like structure function. The left panel shows results for $W = 8$ TeV, while the right panel shows results for $W = 13$ TeV.

D. Role of longitudinal structure function

We now wish to discuss the importance of the longitudinal structure function in the photon-flux. This needs some clarification. Arguably the most physical representation of the inelastic flux would be to write the inelastic flux 2.12 directly in terms of structure functions $F_T(x_{Bj}, Q^2) = 2x_{Bj}F_1(x_{Bj}, Q^2)$ and $F_L(x_{Bj}, Q^2)$. In terms of these structure functions F_2 decomposes as $F_2(x_{Bj}, Q^2) = (F_T(x_{Bj}, Q^2) + F_L(x_{Bj}, Q^2))/(1 + \kappa^2)$, with $\kappa^2 = 4x_{Bj}^2 m_p^2/Q^2$. If we insert this into Eq.(2.12), we get positive contributions from F_T as well as F_L . In practice, we have a wealth of experimental data on F_2 , and much less knowledge of F_L . It is therefore more practical to express the photon flux directly in terms of F_2 and F_L .

We now want to check to which extent the photon fluxes can be evaluated from F_2 only. We therefore evaluate the photon flux for two different cases:

1. in Eq.(2.12) we substitute $2x_{Bj}F_1(x_{Bj}, Q^2) = (1 + \kappa^2)F_2(x_{Bj}, Q^2) - F_L(x_{Bj}, Q^2)$ (denoted as $d\sigma(F_2 + F_L)/dM_{WW}$),
2. in eq.(2.12) we substitute $2x_{Bj}F_1(x_{Bj}, Q^2) = F_2(x_{Bj}, Q^2)$ (denoted as $d\sigma(F_2)/dM_{WW}$).

In Fig.16 we show the ratio $d\sigma(F_2 + F_L)/dM_{WW}/d\sigma(F_2)/dM_{WW}$ for two different energies. In such a decomposition the cross section when both F_2 and F_L are taken into account is smaller by 4-5 % than the cross section when only F_2 is taken into account, independent of M_{WW} .

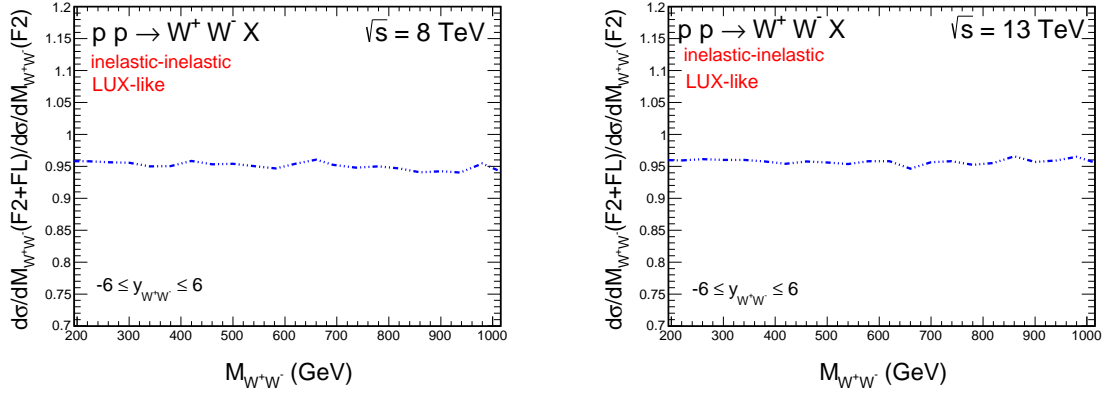


FIG. 16: The role of the longitudinal structure function as a function of W^+W^- invariant mass. Shown is the ratio of the cross section with and without F_L structure function in the unintegrated photon fluxes. The calculation was performed for the LUX-like structure function. The left panel shows results for $\sqrt{s} = 8$ TeV, while the right panel shows results for $\sqrt{s} = 13$ TeV.

E. Rapidity distance between W bosons

The $\gamma\gamma$ contribution is of the order of 2 % for the inclusive cross section as discussed at the beginning of this section. The technical problem is how to measure the $\gamma\gamma$ contribution in experiment. This can be done by imposing an extra condition on the size of the rapidity gaps around the electroweak vertex.

In Fig.17 we show the distribution in the distance in rapidity between the two produced W bosons (dotted line) without any extra condition on rapidity gaps. The distribution is fairly flat over several units. This (rapidity distance between muon and electron) can perhaps be used to enhance the data sample for the $\gamma\gamma \rightarrow W^+W^-$ mechanism. For reference we show also contribution of the $q\bar{q} + \bar{q}q$ annihilation (dash-dotted line) and gluon-gluon fusion (dashed line) which proceed via quark loops. The latter calculation is performed with LoopTools package [32] (for details we refer to [33]). The distribution corresponding to gluon-gluon fusion is much narrower than that of the $\gamma\gamma$ fusion. It is not so for the quark-antiquark annihilation. The latter is broader due to parton distribution product ($q(x_1)\bar{q}(x_2)$, containing valence quarks) as well as due to presence of s -channel photon and Z -boson exchanges. Excluding artificially the latter contributions makes the distribution in Δy much narrower. The distributions change shapes when imposing extra cut on $M_{WW} > 500$ GeV (lower panels), but the general situation is similar.

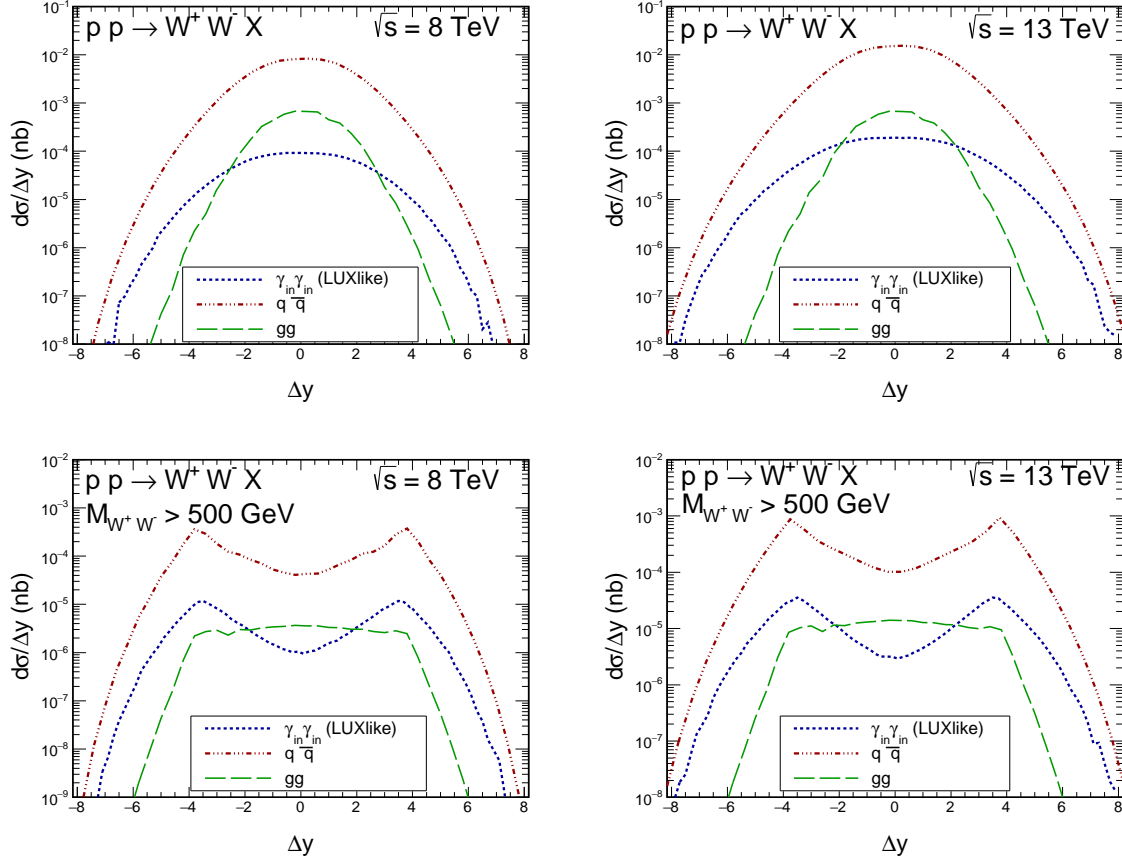


FIG. 17: Distribution in rapidity distance between W bosons. The calculation for the $\gamma - \gamma$ contribution (dotted-line, inelastic-inelastic contribution only) was performed for the LUX-like structure function. The left panel shows results for $\sqrt{s} = 8$ TeV, while the right panel shows results for $\sqrt{s} = 13$ TeV. For comparison we show also contribution of the $q\bar{q}$, $\bar{q}q$ annihilation (dash-dotted line) and $gg \rightarrow W^+W^-$ (dashed line). In the lower panels we show results for extra cut imposed on the invariant mass of the M_{WW} system – $M_{WW} > 500$ GeV.

V. CONCLUSIONS

In the present paper we have discussed the production of W^+W^- pairs created via the photon-photon fusion mechanism. In contrast to previous approaches we include transverse momenta of photons incoming to the hard process. The matrix elements derived in [20] have been used. The explicit dependence on polarization state of W bosons has allowed us to calculate different polarization contributions.

We have obtained cross section of about 1 pb for the LHC energies. This is about 2 % of the total integrated cross section dominated by the quark-antiquark annihilation and gluon-gluon fusion.

Different combinations of the final states (elastic-elastic, elastic-inelastic, inelastic-elastic, inelastic-inelastic) related to whether the incoming protons do or do not undergo dissociation have been considered. We have focused rather on the dominant inelastic-inelastic component.

The unintegrated photon fluxes were calculated based on modern parametrizations of the proton structure functions from the literature.

Several differential distributions in W boson transverse momentum and rapidity, WW invariant mass, transverse momentum of the WW pair have been presented and compared with previous results obtained in the collinear approach in [4]. We have obtained a smaller cross section for large W^+W^- invariant masses than in the collinear approximation. Our predictions may be considered as realistic Standard Model reference in searches of effects beyond Standard Model in the $\gamma\gamma \rightarrow W^+W^-$ process.

Several correlation observables have been studied. Large contributions from the regions of large photon virtualities Q_1^2 and/or Q_2^2 have been found putting in question the reliability of leading-order collinear-factorization approach. We have found larger virtualities for larger invariant masses of the W^+W^- system. This results seems universal and would be similar e.g. for production of charged Higgs H^+H^- pairs via $\gamma\gamma$ fusion.

We have found that x values (arguments of F_2 structure functions) are typically $x \sim 0.1-0.5$. In contrast to the production of charged lepton pairs the production of W^+W^- pairs requires therefore structure functions in the region where they were studied (measured and fitted). The dominant part comes from the region described by the DGLAP evolution equation and only a small fraction comes from nonperturbative region. The nonperturbative contribution (small Q^2 region) was much larger for the charged lepton production [3] where a detailed studies of resonances was necessary.

We have presented a decomposition of the cross section into individual contributions of different polarizations of both W bosons. It has been shown that the TT (both W transversally polarized) contribution dominates and constitutes a little bit more than 80 % of the total cross section. The LL (both W longitudinally polarized) contribution is interesting in the context of studying WW interactions or searches beyond the Standard Model. However, the corresponding cross section is only about 5 %. We have found only a mild dependence of relative amount of different contributions as a function of WW invariant mass.

We have quantified the effect of inclusion of longitudinal structure function into the transverse momentum dependent fluxes of photons. A rather small, approximately M_{WW} - independent, effect was found.

The discussed here $\gamma\gamma \rightarrow W^+W^-$ mechanism leads to rather large rapidity separations of W^+ and W^- boson. It requires further studies to understand whether it can be used to relatively enhance contribution of the $\gamma\gamma \rightarrow W^+W^-$ in experimental studies.

Acknowledgments

We are indebted to Piotr Lebiedowicz for providing us a program to calculate gluon-gluon fusion mechanism. This study was partially supported by the Polish National Science Centre grants DEC-2013/09/D/ST2/03724 and DEC-2014/15/B/ST2/02528 and by the Center for Innovation and Transfer of Natural Sciences and Engineering Knowledge in Rzeszów. We are indebted to Laurent Forthomme for discussion of some issues presented here.

-
- [1] V. M. Budnev, I. F. Ginzburg, G. V. Meledin and V. G. Serbo, Phys. Rept. **15**, 181 (1975).
 - [2] G. G. da Silveira, L. Forthomme, K. Piotrkowski, W. Schäfer and A. Szczurek, JHEP **1502** (2015) 159 [arXiv:1409.1541 [hep-ph]].

- [3] M. Luszczak, W. Schäfer and A. Szczurek, Phys. Rev. D **93**, no. 7, 074018 (2016) [arXiv:1510.00294 [hep-ph]].
- [4] M. Luszczak, A. Szczurek and Ch. Royon, JHEP **02** (2015) 098.
- [5] P. Lebiedowicz and A. Szczurek, Phys. Rev. **D91** (2015) 095008.
- [6] A. D. Martin, R. G. Roberts, W. J. Stirling and R. S. Thorne, Eur. Phys. J. C **39** (2005) 155 [hep-ph/0411040].
- [7] R. D. Ball *et al.* [NNPDF Collaboration], Nucl. Phys. B **877** (2013) 290 [arXiv:1308.0598 [hep-ph]].
- [8] C. Schmidt, J. Pumplin, D. Stump and C. P. Yuan, Phys. Rev. D **93** (2016) no.11, 114015 [arXiv:1509.02905 [hep-ph]].
- [9] F. Giuli *et al.* [xFitter Developers' Team], Eur. Phys. J. C **77** (2017) no.6, 400 [arXiv:1701.08553 [hep-ph]].
- [10] I. F. Ginzburg and A. Schiller, Phys. Rev. D **57**, 6599 (1998) [hep-ph/9802310].
- [11] A. Manohar, P. Nason, G. P. Salam and G. Zanderighi, Phys. Rev. Lett. **117** (2016) no.24, 242002 [arXiv:1607.04266 [hep-ph]].
- [12] A. V. Manohar, P. Nason, G. P. Salam and G. Zanderighi, JHEP **1712** (2017) 046 [arXiv:1708.01256 [hep-ph]].
- [13] E. Chapon, C. Royon and O. Kepka, Phys. Rev. D **81** (2010) 074003 [arXiv:0912.5161 [hep-ph]].
- [14] T. Pierzchala and K. Piotrkowski, Nucl. Phys. Proc. Suppl. **179-180**, 257 (2008) [arXiv:0807.1121 [hep-ph]].
- [15] V. Khachatryan *et al.* [CMS Collaboration], JHEP **1608**, 119 (2016) [arXiv:1604.04464 [hep-ex]].
- [16] M. Aaboud *et al.* [ATLAS Collaboration], Phys. Rev. D **94**, no. 3, 032011 (2016) [arXiv:1607.03745 [hep-ex]].
- [17] W. Kilian, T. Ohl, J. Reuter and M. Sekulla, Phys. Rev. D **93**, no. 3, 036004 (2016) [arXiv:1511.00022 [hep-ph]].
- [18] R. L. Delgado, A. Dobado and F. J. Llanes-Estrada, Eur. Phys. J. C **77**, no. 4, 205 (2017) [arXiv:1609.06206 [hep-ph]].
- [19] M. Szleper, arXiv:1412.8367 [hep-ph].
- [20] O. Nachtmann, F. Nagel, M. Pospischil and A. Utermann, Eur. Phys. J. C **45**, 679 (2006) [hep-ph/0508132].
- [21] J. Alwall *et al.*, JHEP **1407** (2014) 079 [arXiv:1405.0301 [hep-ph]].
- [22] H. Abramowicz, E. M. Levin, A. Levy and U. Maor, Phys. Lett. B **269** (1991) 465.
- [23] H. Abramowicz and A. Levy, hep-ph/9712415.
- [24] P. E. Bosted and M. E. Christy, Phys. Rev. C **77**, 065206 (2008) [arXiv:0711.0159 [hep-ph]].
- [25] A. Airapetian *et al.* [HERMES Collaboration], JHEP **1105**, 126 (2011) [arXiv:1103.5704 [hep-ex]].
- [26] K. Abe *et al.* [E143 Collaboration], Phys. Lett. B **452**, 194 (1999) doi:10.1016/S0370-2693(99)00244-0 [hep-ex/9808028].
- [27] A. D. Martin, W. J. Stirling, R. S. Thorne and G. Watt, Eur. Phys. J. C **63**, 189 (2009) [arXiv:0901.0002 [hep-ph]].
- [28] A. Szczurek and V. Uleshchenko, Eur. Phys. **C12** (2000) 663; Phys. Lett. **B475** (2000) 120.
- [29] M. Drees and D. Zeppenfeld, Phys. Rev. D **39**, 2536 (1989). doi:10.1103/PhysRevD.39.2536
- [30] S. Chatrchyan *et al.* [CMS Collaboration], Phys. Lett. B **699**, 25 (2011) [arXiv:1102.5429 [hep-ex]].

- [31] G. Aad *et al.* [ATLAS Collaboration], Phys. Lett. B **712**, 289 (2012) [arXiv:1203.6232 [hep-ex]].
- [32] T. Hahn and M. Perez-Victoria, Comput. Phys. Commun. **118** (1999) 153 [hep-ph/9807565].
- [33] P. Lebiedowicz, R. Pasechnik and A. Szczurek, Nucl. Phys. B **867** (2013) 61 [arXiv:1203.1832 [hep-ph]].